INTERFACIAL BEHAVIOR IN SYSTEMS TYPE IV

Andrés Mejía * and Hugo Segura

Group of Thermodynamics. Department of Chemical Engineering, Universidad de Concepción, POB 160-C, Fax : 56-41-247491, Concepción, Chile.

* To whom correspondence should be addressed. Email : amejia@diq.udec.cl

ABSTRACT

Mixtures Type IV exhibit two heteroazeotropic lines, one at low temperature and the other meeting the supercritical range, characterized by the proximity of their critical end points (CEPs). Between these CEPs, the liquid phase is homogeneous inside a narrow range of temperature. The aim of this work is to analyze interface properties and wetting transitions for mixtures Type IV. Interfacial tensions have been calculated by means of the gradient theory, applied to binary van der Waals fluids. This approach is able to predict interfacial tension and phase equilibrium using a common equation of state (EOS).
Results show that interfacial properties and wetting conditions are governed by the densities and the number of phases involved in equilibrium, an scenario that changes as temperature evolves from the low to the high temperature heteroazeotropic line.

Keywords : Interface tension, Gradient Theory, Type IV behavior.

Introduction

Coexisting bulk fluid phases in thermodynamical equilibrium are connected by an interfacial fluid, whose concentration ρ, varies spatially between its bulk fluid phases. Figure 1 shows, schematically, the typical patter of ρ as a function of a spatial coordinate z, for a liquid in equilibrium with its vapor. For mixtures, the interfacial fluid may be enclosed by gas/liquid, liquid/liquid, or gas/liquid/liquid bulk fluids, and its $\rho(z)$ behavior is a function of pure fluids and their bulk densities. In fact, $\rho(z)$ may be or not a monotonic function, as illustrated in Figure 2. From a practical view point, these kinds of interfaces are present in many chemical and environmental processes. For example, interface fluids are presented in heat transfer under boiling conditions, generation of tropospheric ozone, liquid extraction processes, production of herbicides and pesticides, process of enhanced oil recovery, fluids wetting, etc. Therefore, the analysis of interface fluid properties, such as interfacial tension and wetting transitions, are the precise piece to understand and design these industrial processes. In this context, one of the most successful approaches is the square gradient theory of van der Waals [1]. Briefly, the gradient theory (GT) describes a continuous evolution of the density of the Helmholtz energy of an inhomogeneous fluid along the interface, from which the interfacial concentration profile and interface tension can be calculated. It should be noted that the main advantages of the GT approach are the facts that the interfacial behavior is described in the same terms than thermodynamical equilibrium variables, like temperature, pressure and mole fraction, and that the same equation of state (EOS) model can be used to predict both the interfacial behavior and the phase equilibrium conditions. As follows from Rowlinson and Widom [1], the topology of an interface fluid is governed by the type of fluids and their phase equilibria, therefore mixtures with several phase equilibria patterns are adequate candidates to obtain a global understanding of interfacial behavior. Following the van Konynenburg and Scott's work [2], mixtures Type IV are an interesting choice due to the fact these mixtures exhibit two heteroazeotropic lines (one at low and the other at high temperature) which are characterized by their critical end points (CEPs). The main scope of this work is to analyze interface properties and wetting transitions for this kind of mixtures in a planar interface. Our predictions are based on GT applied to the van der Waals EOS (vdW-EOS) with quadratic mixing rule (QMR). The results will be illustrated considering the behavior of the spatial variation of the fluid concentrations along the interface length and the dependence of the interfacial tension on equilibrium conditions.

Theory

The square gradient theory for planar interfaces

The gradient theory (GT) was originally developed by van der Waals in 1894 and reformulated later by Cahn and Hilliard in 1958 [3]. In this approach, the interfacial tension between two bulk phases (α, β) is related to the interface length by the following equation [1]:

$$\sigma = 2\int_{-\infty}^{\infty}\left(\Phi + P^0\right)dz = 2\int_{-\infty}^{\infty}\Delta\Phi\, dz \tag{1}$$

where σ is the interfacial tension, P^0 is the bulk equilibrium pressure, z is a coordinate normal to the interface. The integral limits describe the boundary conditions of fluid phases, i.e ρ_i ($z = +\infty$) = ρ_i^{α} and ρ_i ($z = -\infty$) = ρ_i^{β} where $\rho_i^{\alpha,\beta}$ corresponds to the molar concentration of component i in the α and β bulk phases, respectively. Finally, Φ is the grand thermodynamic potential, which is defined as:

$$\Phi\left[\rho_i, \rho_m\right] = a_0\left[\rho_i, \rho_m\right] - \sum_{i=1}^{n_c}\rho_i\mu_i^0\left[T^0, V^0, \rho_i^0\right] \tag{2}$$

In Eq. 2 ρ_m is concentration of the mixture which is related to the concentration of species, ρ_i, and the mole fraction x_i by $\rho_i = x_i\,\rho_m$. n_c stands for the number of components. V^0, T^0, ρ_i^0 are the equilibrium volume, temperature and concentration of component i, respectively. a_0 is the density of the Helmholtz energy of the homogeneous system ($a_0 = A/V$) and μ_i^0 is the chemical potential of component i at equilibrium. Both a_0 and μ_i^0 can be determined directly from any EOS. In Appendix, we summarize these expressions for the vdW-EOS with QMR. An important feature of the Φ function, as stated by Rowlinson and Widom [1], is that the $\Delta\Phi$ vs. ρ_m projection allows to establish if the phase equilibria exhibits stable phases (absolute minimums) or metastable phases (relative minimums). An example of absolute and relative minimums at $\Delta\Phi$ - ρ_m projection can be observed in Figure 3.
Replacing Eq. 2 in 1 reveals that the integration processes needs an additional relation between ρ_i and z. Following the GT, this relation is given by the following set of partial differential equations (PDE) [6] :

$$\sum_{j=1}^{n_c} c_{ij}\frac{d\rho_j^2}{dz^2} - \frac{1}{2}\sum_{k,j=1}^{n_c}\frac{\partial c_{kj}}{\partial\rho_i}\frac{d\rho_k}{dz}\frac{d\rho_j}{dz} = \frac{\partial\Phi}{\partial\rho_i} \tag{3}$$

where $i = 1,..n_c$

$$\rho_i\big|_{z=-\infty} = \rho_i^{\alpha} \qquad \text{and} \qquad \rho_i\big|_{z=\infty} = \rho_i^{\beta}$$

where c_{ij} is the cross influence parameter ($c_{ij} = c_{ji}$). Theoretically, c_{ij} is related to the mean square range of the direct correlation function of an homogeneous fluid. c_{ij} is given by [7]

$$c_{ij}\left(\rho, T\right) = \frac{\kappa T N_{av}^2}{6}\int_V s^2 c_0^{ij}\left(s;\rho\right)d^3s \tag{4}$$

In this expression κ is the Boltzmann's constant, N_{av} is the Avogadro's constant, s is a characteristic coordinate between species i and j, and c_o^{ij} (s ;ρ) is the two body direct correlation function between species i and j in homogeneous fluids. However, since c_o^{ij} (s ;ρ) is intractable, some approximation has been applied [6]. One of the most successful approximation is c_o^{ij} (s) [8], which automatically transforms the PDEs to a set of ordinary differential equations (ODEs). Based on c_o^{ij}'s approximation, c_{ij} for pure fluids is given by [8]:

$$c_{ii}(T) = -\frac{N_{av}^2}{6}\int_V s^2 u(s) g(s) d^3 s \tag{5}$$

where u is the intermolecular potential and g is the radial distribution function. For the fluids studied here (vdW fluids), the Sutherland potential is used for u, and g is taken as a step function. u and g are given by:

$$u_{ii}(s) = -\varepsilon_{ii}\left(\frac{\sigma_{ii}}{s}\right)^6 \quad ; \quad g_{ii}(s) = \begin{cases} 0 \text{ if } s < \sigma_{ii} \\ 1 \text{ if } s \geq \sigma_{ii} \end{cases} \tag{6}$$

ε_{ii} and σ_{ii} represent length and energy parameters characteristic of molecular interactions of specie i. Replacing Eqs. 6 in 5 and integrating over V, c_{ii} takes the form:

$$c_{ii}(T) = \frac{2}{3} N_{av}^2 \pi \varepsilon_{ii} \sigma_{ii}^5 \tag{7}$$

Following Carey's work, Eq. 7 can be conveniently rewritten in terms to a_{ii} and b_{ii} as

$$\frac{c_{ii}}{a_{ii} b_{ii}^{2/3}} = \left(\frac{3}{2\pi N_{av}}\right)^{2/3} \tag{8}$$

For the case of mixtures, c_{ij} can be obtained by averaging the pure component influence parameters according to the following geometric combining rule [6]

$$c_{ij} = (1 - \chi_{ij})\sqrt{c_{ii} c_{jj}} \tag{9}$$

where χ_{ij} is an adjustable parameter, obtained by fitting experimental data of σ for mixtures. However, as some authors have been shown [6, 9], selected $\chi_{ij} = 0$ is a good choice for several fluid/fluid interfaces. The advantages of $\chi_{ij} = 0$ are that c_{ij} can be predicted from pure fluids information, and the ODEs become to the following system of algebraic equations (AEs) [6]:

$$\sqrt{c_{ss}}\left[\mu_k(\rho)-\mu_k^0\right]=\sqrt{c_{kk}}\left[\mu_s(\rho)-\mu_s^0\right] \qquad k = 1, 2, ..., s-1, s+1, ..., n_c \qquad (10)$$

These AEs can be solved by setting a value of ρ_s and calculating the ρ_k values. Once ρ_k (ρ_s) have been determined, the ρ_k (z) projections are calculated from the ODEs, which after some algebra yields to [6,9] :

$$z(\rho_s)-z_0\left(\rho_s^0\right)=\int_{\rho_s^0}^{\rho_s}\sqrt{\frac{1}{2\Delta\Phi}\sum_{i,j=1}^{n_c}c_{ij}\left(\frac{d\rho_i}{d\rho_s}\right)\left(\frac{d\rho_j}{d\rho_s}\right)}\,(d\rho_s) \qquad s = 1, 2, ..., n_c \qquad (11)$$

where z_0 is a reference of z coordinate, where $\rho = \rho_s^0$. Some patterns of ρ_k (z) projections were shown for pure fluids and mixtures in Figures 1 and 2, respectively. Eq. 11 also brings the possibility to express σ in terms to ρ rather than z. Replacing it in Eq. 1, σ (ρ) is given by :

$$\sigma=\int_{\rho_s^\alpha}^{\rho_s^\beta}\sqrt{2\Delta\Phi\sum_{i,j=1}^{n_c}c_{ij}\left(\frac{d\rho_i}{d\rho_s}\right)\left(\frac{d\rho_j}{d\rho_s}\right)}\,d\rho_s \qquad (12)$$

The latter transformation is useful to understand the σ behavior near to critical states, and the wetting transition of interface fluids, as we will describe in the following section. It is well known that when two phases (α, β) are approaching to their critical state $\rho^\alpha \approx \rho^\beta$, therefore Eq. 12 produces $\sigma \to 0$. For the case to three phases (α, β, γ), with $\rho^\alpha \neq \rho^\beta \neq \rho^\gamma$ along to $\alpha\beta\gamma$E, interfacial tensions are deferments $\sigma_{\alpha\beta} \neq \sigma_{\alpha\gamma} \neq \sigma_{\beta\gamma}$ but near to a CEP $\rho^\alpha \neq \rho^\beta \approx \rho^\gamma$ which conduces to $\sigma_{\alpha\beta} \approx \sigma_{\alpha\gamma}$ and $\sigma_{\beta\gamma} \to 0$.

Wetting transitions at fluid interfaces

Considering Figure 3 and following the structure of Eq. 12, we can conclude that the area below two bulk phases is proportional to σ, and in general when π different phases are in equilibrium, [½ (π – 1) π] independent σs can be formed and are interrelated via their contact angles [1]. For the cases studied here two (α, β) and three (α, β, γ) phases in equilibrium, consequently we have one ($\sigma_{\alpha\beta}$) or three ($\sigma_{\alpha\beta}$, $\sigma_{\alpha\gamma}$, $\sigma_{\beta\gamma}$) different interfacial tensions, respectively. In the later case, σs are interrelated by [1] :

$$\sigma_{\alpha\beta} < \sigma_{\alpha\gamma} + \sigma_{\beta\gamma} \qquad \textit{Neumman inequality} \qquad (13.a)$$

$$\sigma_{\alpha\beta} = \sigma_{\alpha\gamma} + \sigma_{\beta\gamma} \qquad \textit{Antonow rule} \qquad (13.b)$$

and cyclic permutation of α, β, and γ. The situation described by Eq. 13.a is called partial wetting of γ phase in $\alpha\beta$ interface. Eq. 13.b denotes the total wetting of the γ phase in $\alpha\beta$ interface, and the transition from partial to total wetting (or vice versa) is called *Wetting*

transition [1], which can occur at certain point along to three phase equilibrium ($\alpha\beta\gamma E$) line. The evolution of $\sigma_{\alpha\beta}$ along to $\alpha\beta\gamma E$ is schematically illustrated in Figure 4.

Results and Discussion

Based on the Global Phase Equilibria for the vdW-EOS [2], we select a typical mixture Type IV. Table I summarizes the critical properties of pure components and the interaction parameter for this mixture. Figure 5 illustrates its pressure – temperature diagram, which exhibits three critical lines, and two heteroazeotropic lines, as expected. Specific details related to the Type IV and its construction can be found in Konynenburg and Scott [2] and Rowlinson and Swinton [10]. In order to describe the interfacial behavior related to Figure 5, we need to consider the topological evolution of interfacial projections (i.e $\Delta\Phi - \rho_m$, $\rho - z$, and $\sigma - P$, x) in the subcritical phase equilibriums related to this Type. Using the temperature as a variable we are able to collect all subcritical equilibriums in four zones. Table II summarizes these zones, their temperature ranges and the isothermal conditions which will be used to analyze the interfacial behavior.
In the approximation presented here, all interfacial calculations were performed using $\chi = 0$. The advantage of $\chi = 0$ is that GT acquires a predictive character without a lost of generality [11, 12]. Details related to the interfacial calculations are summarized in Figure 6. However, it is important to establish that for cases where $\chi \in (0; 1)$ and $n_c > 2$ more sophisticated algorithms need to be considered [6, 9].
In the following section we describe the interfacial topology in terms to the interfacial projections in the whole mole fraction range. We divide our analysis in two sections, one is related to the variation of the interfacial projections for each zone of Type IV mixture (see Table II) and the other is consider wetting transitions along the two heteroazeotropic lines.

Evolution of interface properties with the temperature.

Figures 7 depict the behavior of the $\Delta\Phi - \rho_m$ profile at the four zones for the whole mole fraction range. From these figures, we can observe that each isothermal projection displays only two absolute minimums for a fixed mole fraction. This fact confirms that two bulk fluid phases (GL or LL) are present at the temperature for which the fluid/fluid equilibria has been calculated, as we can expect from the theory and Table II. Additionally, Figures 7 also show some relative minimums near to CEPs which are due to the fact that an embryo phase (γ) is present. As is expected, the position and magnitude of γ changes as T or x_i changes. For example, for an isothermal condition, γ changes from an embryo state to an equilibria state (see Figure 7.a, c) as x_i increases. At a fixed x_i, the density of γ may changes from liquid like to gas like densities as T increases. In additions, from the theory arguments, we can anticipate, from $\Delta\Phi - \rho_m$ diagrams, that no always σ_{GL} is greater than σ_{LL}. The σ value depends on the thermomecanics conditions at which the equilibrium is calculated.

Figures 8 illustrate the concentration of species along the interface length. These $\rho - z$ projections were calculated at the same thermodynamical conditions than Figure 7. Inspections on these diagrams revels that the more volatile component (1) always shows a stationary point (SP), where its concentration is larger than the bulk concentration. This fact reflects that (1) is positively absorbed at the interface. Moreover, the less volatile component (2) is not absorbed. From these Figures we can observe that the position and magnitude of SPs changes as T or x_i changes. In fact, we can conclude that both position and magnitude of SPs increases as x_i increases. For a fixed x_i, the position of SPs increases and the magnitude decreases as T increases. Figures 8 also show that LL interfaces exhibit smoother profiles and larger interface widths than GL interfaces. This behavior is caused, mainly, by the bulk concentration gradient in a LLE and in a GLE. Finally, when previous patterns are compared with computer simulations [13] we can conclude that $\rho - z$, from GT, shows a good qualitative agreement to that simulations for LL and GL interfaces.
Figures 9 show the σ - P projections at the same isothermal conditions considering in Figures 7 and 8. As expected from Table II, one or three interfacial tensions (σ_{GL} or σ_{GL1} σ_{L1L2} σ_{GL2}) are presented in these σ (P) diagrams. A quick inspection of each isothermal σ - P diagram revels that, in general, σ decreases as the phase equilibrium tends to the critical point, as expected from Eq. 12. However a close view shows that σ may be increased in regions where the γ phase is presented. The σ (P) behavior can be summarized as follows : σ is not a continuous function in zones 1 and 3, its discontinuity is due to the fact that three equilibria condition are present into these zones (see Table II). In particular, zone 1 shows that σ_{GL1}, $_{GL2} > \sigma_{L1L2}$. zone 3 shows two regimes as the temperature increases. From T_{LCEP2} / T_{c1} to $T / T_{c1} = 1$, σ (P) is similar than zone 1. From $T / T_{c1} = 1$ to T_{UCEP2} / T_{c1} $\sigma_{GL1} > \sigma_{L1L2} > \sigma_{GL2}$. For zones 2 and 4 σ is a continuous function of P, however its trend is affected by the presence of the γ phase. In order to complete the σ descriptions in zones 1 to 4, Figures 10 collect the evolution of the interfacial tension on mole fraction σ (x). From these Figures we can observe similar patterns discussed previously. Regrettably, no experimental information are available to contrast our σ (P, x) predictions. However, we can observe that our description reflects the facts to their phase diagrams, and following the same patters observed by other authors [9]

Wetting transitions along to three phase equilibria

Figures 11 show the $\sigma - T$ projections along to the two three phase equilibria for the mixture Type IV, and Table III summarizes its behavior as temperature increases. From Table III, we can establish that at a CEP three phase equilibria converges, simultaneously, to one subcritical equilibria and one critical equilibria. These interfacial tension results agree to the phase description from van Konynenburg and Scott. In addition, from these Figures and Eqs. 13, we can conclude that along to $[GLL]_1$ line, wetting transitions never occur. But along to $[GLL]_2$, $\sigma_{GL2} = \sigma_{GL1} + \sigma_{L2L1}$ at $T / T_{c1} = T_w / T_{c1} = 0.9153$, and therefore, the $[GLL]_2$ line exhibits a wetting transition. Physically, this transition means that of the GL_2 interface, a layer of a second liquid phase (L_1) intrudes between G and L_2 phases. In complement, it is important to state that $\Delta\Phi(\rho_m)$ and $\rho(z)$ show the expected

behavior of a three phase equilibrium (see Figures 2 and 3). These behavior reinforce the phase and interface patterns previously described.

Concluding Remarks

In this work we analyze interfacial properties and wetting transitions for mixtures Type IV using the GT and the vdW-EOS with QMR. The advantage of this approach is that a common EOS can be used to predict phase equilibrium as well as interfacial properties. This advantage bring the possibility to explain the phase equilibria and its stability from the interfacial behavior. According to results, interfacial properties and wetting conditions are governed by the densities and the number of phases involved in equilibrium, an scenario that changes as temperature evolves from the low to the high temperature heteroazeotropic line.

Acknowledgments

This work was financed by FONDECYT, Santiago, Chile (Project 2010100).

References

[1] Rowlinson, J. S. ; Widom, B. **1982**, "*Molecular Theory of Capillarity*," Oxford University Press, Oxford.

[2] van Konynenburg, P. ; Scott, R. *Phil. Trans. Royal Society (London)* **, 1980**, *298* A, 495

[3] Cahn, J.W. ; Hilliard, J.E. *J. Chem. Phys.,* **1958**, *28*, 258

[4] Van Ness, H., Abbott, M. **1982**, "*Classical Thermodynamics of Nonelectrolyte Solutions,"* McGraw-Hill, New York.

[5] Wisniak, J. ; Apelblat, A. ; Segura, H. *Chem. Eng. Sci.*, **1998**, *53*, 743

[6] Carey, B.S. The Gradient Theory of Fluid Interfaces, Ph.D. Thesis, **1979**, University of Minnesota.

[7] Bongiorno, V. ; Scriven, L.E. ; Davis, H.T. *J. Colloid Interface Sci.,* **1976**, *57*, 462

[8] McCoy, B. F. ; Davis, H. T. *Phys. Rev. A.,* **1979**, *20*, 1201

[9] Cornelisse, P. M. W. The Gradient Theory Applied, Simultaneous Modelling of Interfacial Tension and Phase Behaviour, Ph.D. Thesis, **1997**, Delft University.

[10] Rowlinson, J. S. ; Swinton, F. L. *Liquids and Liquid Mixtures* ; Butterworths : London, 1982.

[11] Sullivan, D. E. *J. Chem. Phys*., **1982**, *77*, 2632

[12] Costas, M. E. ; Vera, C. ; Robledo, A. *Phys. Rew. Lett*. **1983**, *51*, 2394.

[13] Winkelmann, J. *J. Phys. : Condens. Matter.,* **2001** *13*, 4739

Table I. Critical properties of pure components and interaction parameter

T_{c2} / T_{c1}	P_{c2} / P_{c1}	k_{12}
3.9692	6.1429	-0.3655

Table II. Classification of subcritical phase equilibria, and isothermal conditions for the interfacial analyze.

Zone	*Temperature Range* (T/T_{c1})	*Equilibria Type*	*Selected Temperature* (T/T_{c1})
1	0 to 0.7966 (T_{UCEP1})	GL_1, GL_2, L_1L_2	0.78
2	0.7966 to 0.8457 (T_{LCEP2})	GL	0.82
3	0.8457 to 1.0549 (T_{UCEP2})	GL_1, GL_2, L_1L_2	0.95
4	1.0549 to 3.9692 (T_{c2})	GL	1.10

Table III. Interfacial tension behavior along three phase equilibria for mixture Type IV

$[GLL]_1$

Temperature Range	*Phase Equilibria Type*	*Interfacial tension behavior*
$T < T_{UCEP1}$	*subcritical equilibria*	
	GL_1, L_1L_2	σ decreases as T increases
	GL_2	σ increases as T increases
$T = T_{UCEP1}$	*subcritical equilibria*	
	$GL_1 = GL_2$	$\sigma_{GL1} = \sigma_{GL2} \neq 0$
	critical equilibria	
	L_1L_2	$\sigma_{L1L2} = 0$

$[GLL]_2$

Temperature Range	*Phase Equilibria Type*	*Interfacial tension behavior*
$T = T_{LCEP2}$	*subcritical equilibria*	
	$GL_1 = GL_2$	$\sigma_{GL1} = \sigma_{GL2} \neq 0$
	critical equilibria	
	L_1L_2	$\sigma_{L1L2} = 0$
$T_{LCEP2} < T < T_{UCEP2}$	*subcritical equilibria*	
	GL_1, GL_2, L_1L_2	σ_{GL1} first decreases and then increases, σ_{L1L2} decreases and σ_{GL2} increases as T increases
$T = T_{UCEP2}$	*subcritical equilibria*	
	$GL_1 = L_1L_2$	$\sigma_{GL1} = \sigma_{L1L2} \neq 0$
	critical equilibria	
	GL_2E	$\sigma_{GL2} = 0$

Appendix. Density of the Helmholtz energy of the homogeneous system (a_o) and chemical potential of component i (μ_i^0) from van der Waals equation of state.

The van der Waals equation of state (vdw-EOS) is given, in terms to P(T,ρ), by :

$$P = \frac{RT\rho}{1-\rho b} - a\rho^2 \tag{A.1}$$

where R is the gas constant, a is the cohesion parameter and b is the covolume that, for pure fluids, are given by the following expressions [4] :

$$a_{ii} = \frac{27}{64}\frac{\left(RT_{c,i}\right)^2}{P_{c,i}} = \frac{2}{3}N_{av}^2\pi\varepsilon_{ii}\sigma_{ii}^3 \quad ; \quad b_{ii} = \frac{1}{8}\frac{RT_{c,i}}{P_{c,i}} = \frac{2}{3}N_{av}\pi\sigma_{ii}^3 \tag{A.2}$$

N_{av} is the Avogadro constant, $P_{c,i}$ and $T_{c,i}$ are the critical pressure and the critical temperature for component i. ε_{ii} and σ_{ii} represent length and energy parameters characteristic of molecular interactions of specie i. Eqs. A.2 are extended to mixtures using the QMR. a and b of the mixture are given by :

$$\rho_m^2 a_m = \sum_{i,j=1}^{n_c}\left(1-k_{ij}\right)\rho_i\rho_j\sqrt{a_{ii}a_{jj}} \quad ; \quad \rho_m b_m = \sum_{i=1}^{n_c}\rho_i b_{ii} \tag{A.3}$$

where k_{ij} is the interaction parameter. a_0 and μ_i^0 can be calculate by used the following relations [4,5] :

$$\frac{a_0}{\rho RT} = \int_0^{\rho}\left(\frac{P}{RT\rho^2} - \frac{1}{\rho}\right)d\rho + \frac{1}{\rho}\sum_{i=1}^{n_c}\rho_i \ln\rho_i \quad ; \quad \mu_i^0 = \left(\frac{\partial a_0}{\partial \rho_i}\right)_{T,\rho_j} \tag{A.4}$$

For the case of the vdW-EOS applied to a multi-component fluid, Eqs. A.4 conducted to :

$$a_o = -a_m\rho_m^2 - RT\rho_m \ln\left(1-b_m\rho_m\right) - RT\sum_{i=1}^{nc}\rho_i \ln\left(\frac{P_{ref}}{RT\rho_i}\right) \tag{A.5}$$

$$\mu_i^0 = -RT\ln\left(1-b_m\rho_m\right) + \frac{b_i RT\rho_m}{\left(1-b_m\rho_m\right)} - 2\sum_{j=1}^{nc}a_{ij}\rho_j - RT\ln\left(\frac{P_{ref}}{RT\rho_i}\right) + RT \tag{A.6}$$

where P^{ref} is some freely chosen reference pressure.

Figure Captions

[1] Schematically representation of $\rho - z$ projection for a planar vapor/liquid interface of a pure fluid at the boiling point. (●) VLE bulk densities.

[2] Typical $\rho - z$ projections for mixture. (—) GL_1E, (– – –) GL_1E with adsorption of species on the interfacial zone, (–•–) L_1L_2E, (–••–) GL_1L_2E, (●) liquid bulk density, (○) vapor bulk density.

[3] Usual $\Delta\Phi - \rho_m$ projections at fluid phase equilibria. (—) $\alpha\beta E$, (–•–) $\alpha\beta E$ with an embryo phase, γ, (–••–) $\alpha\beta\gamma E$, (●) absolute minimums (stable phases bulk densities), (○) relative minimums (metastable phases).

[4] Schematically representation of *Wetting transition* along three phase equilibria. α, β, γ phases. (–•–) three phase equilibria ($\alpha\beta\gamma E$), (●) CEP (critical end point), (○) wp (wetting point)

[5] Pressure – Temperature diagram for mixture Type IV. (—) critical line, (•••) vapor pressure, (–••–) GLLE

[6] Block diagram for algorithm calculations

[7] $\Delta\Phi - \rho_m$ projections at several isothermal conditions. (—) $x_1 = 0.25$, (–•–) $x_1 = 0.50$, (–••–) $x_1 = 0.75$, (●) VLE bulk densities.

[8] $\rho - z$ projections at several isothermal conditions. (–•–) ρ_1, (–••–) ρ_2, (●) VLE bulk densities, (○) stationary points (sp)

[9] $\sigma - P$ diagrams at several isothermal conditions. (●) end points

[10] $\sigma - x$ diagrams at several isothermal conditions. (●) end points

[11] $\sigma - T$ diagrams along $[GLL]_1$ and $[GLL]_2$

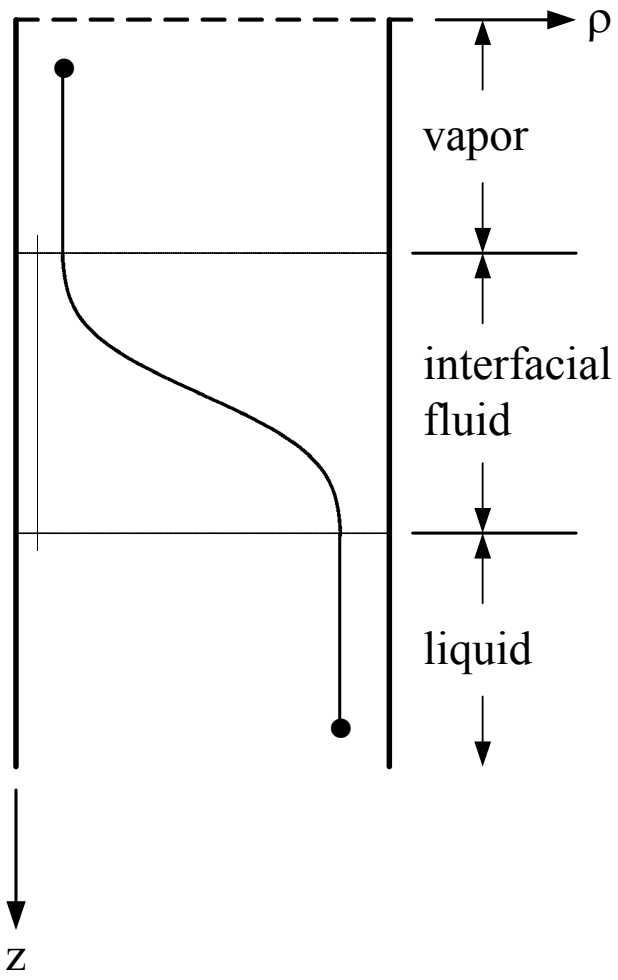

Figure 1

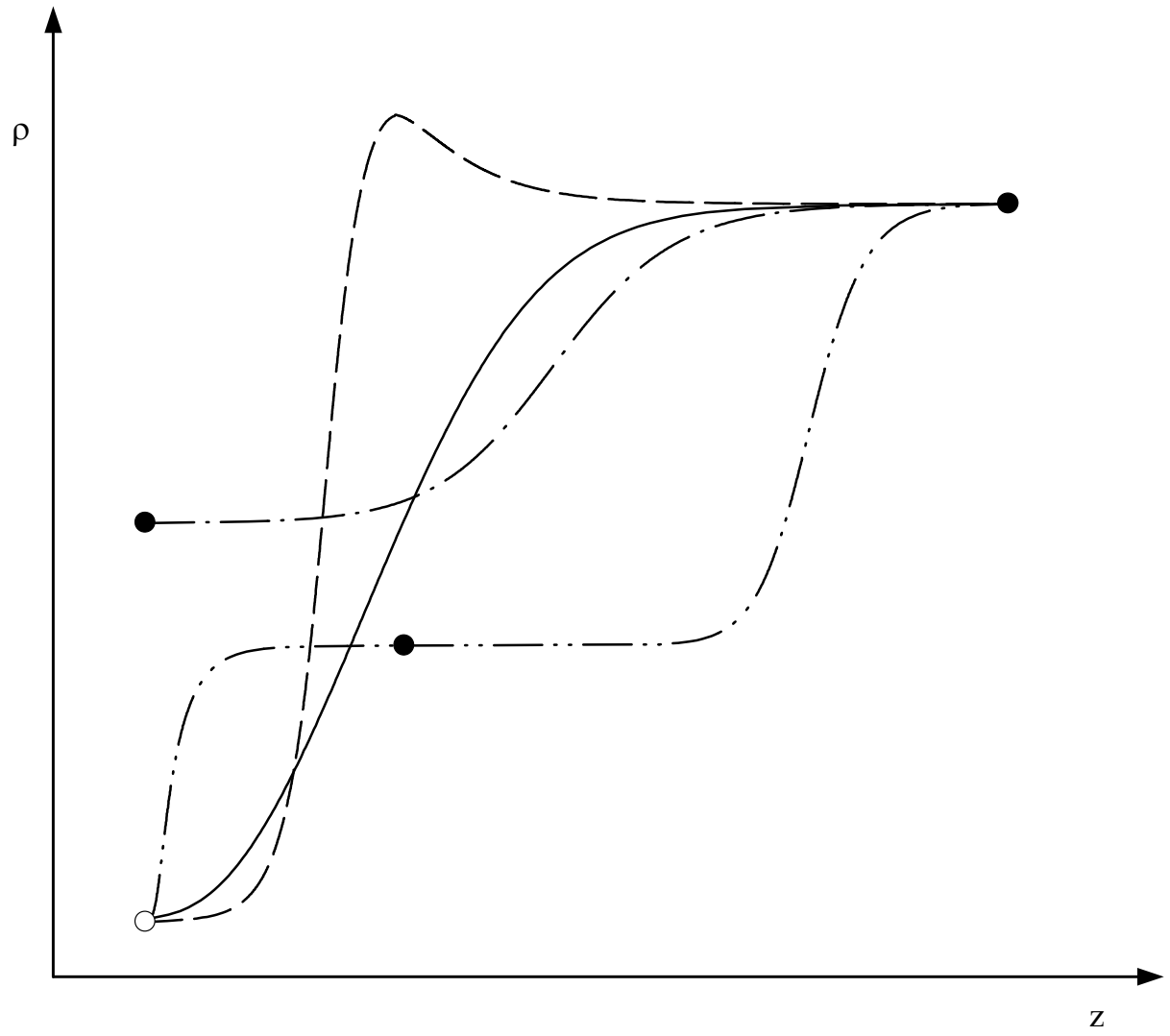

Figure 2

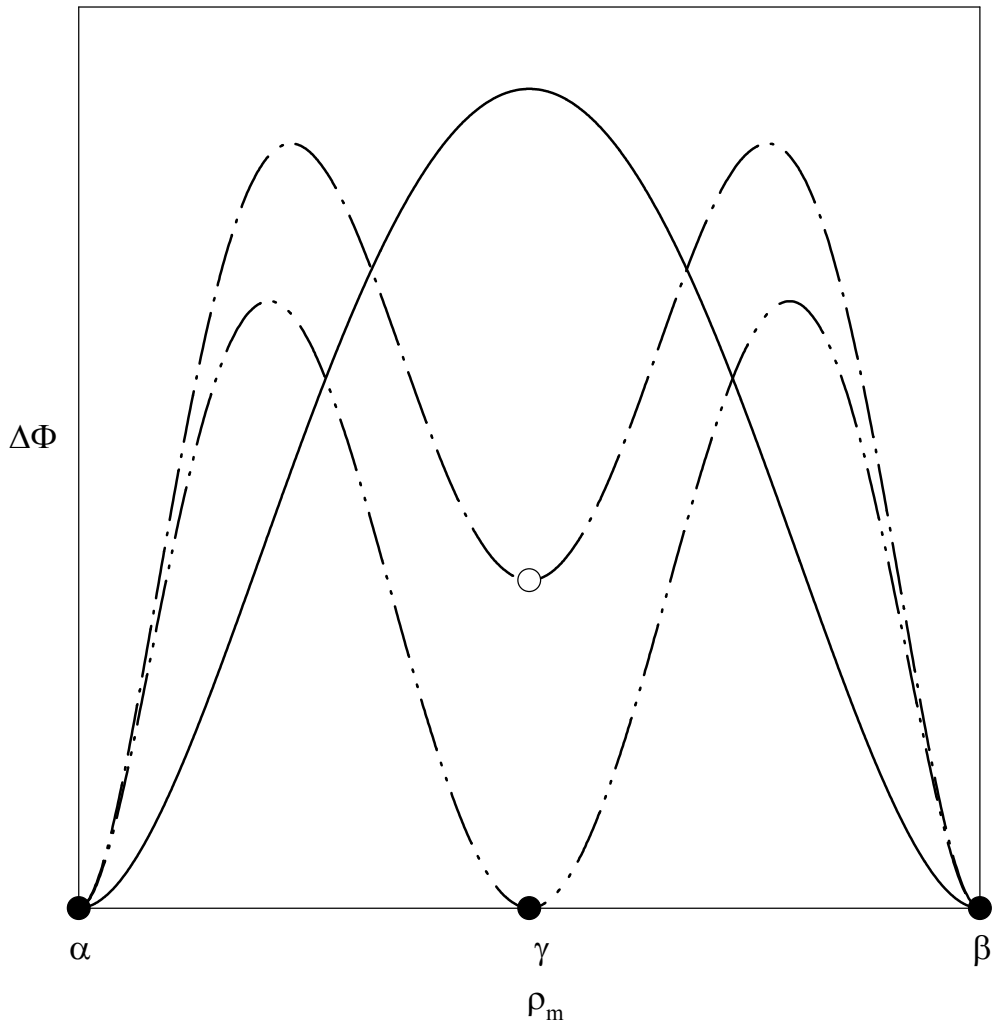

Figure 3

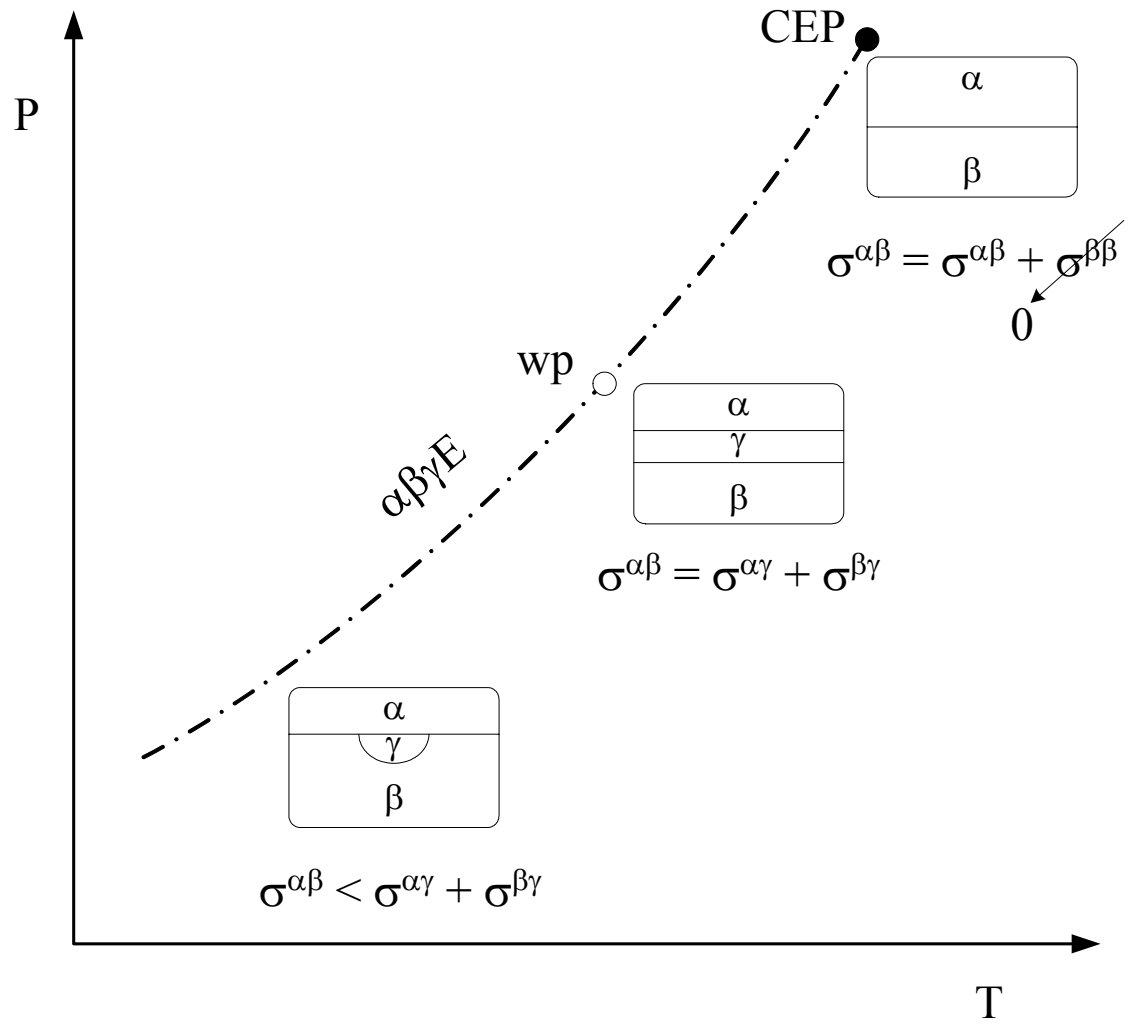
CEP
P
α
β
$\sigma^{\alpha\beta} = \sigma^{\alpha\beta} + \sigma^{\beta\beta}$
0
wp
α
γ
β
αβγE
$\sigma^{\alpha\beta} = \sigma^{\alpha\gamma} + \sigma^{\beta\gamma}$
α
γ
β
$\sigma^{\alpha\beta} < \sigma^{\alpha\gamma} + \sigma^{\beta\gamma}$
T

Figure 4

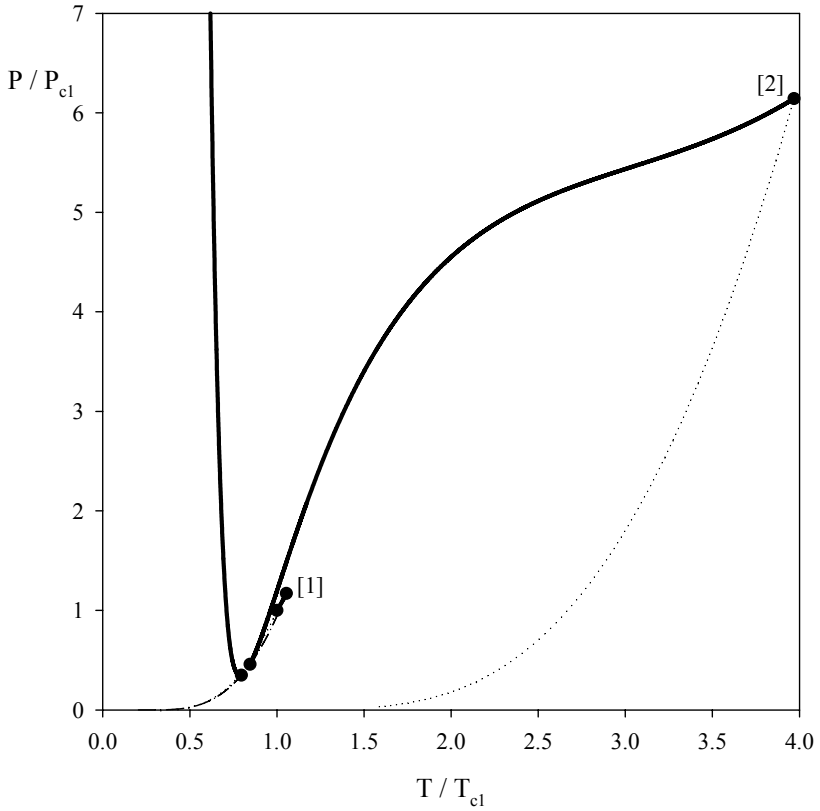

Fig. a

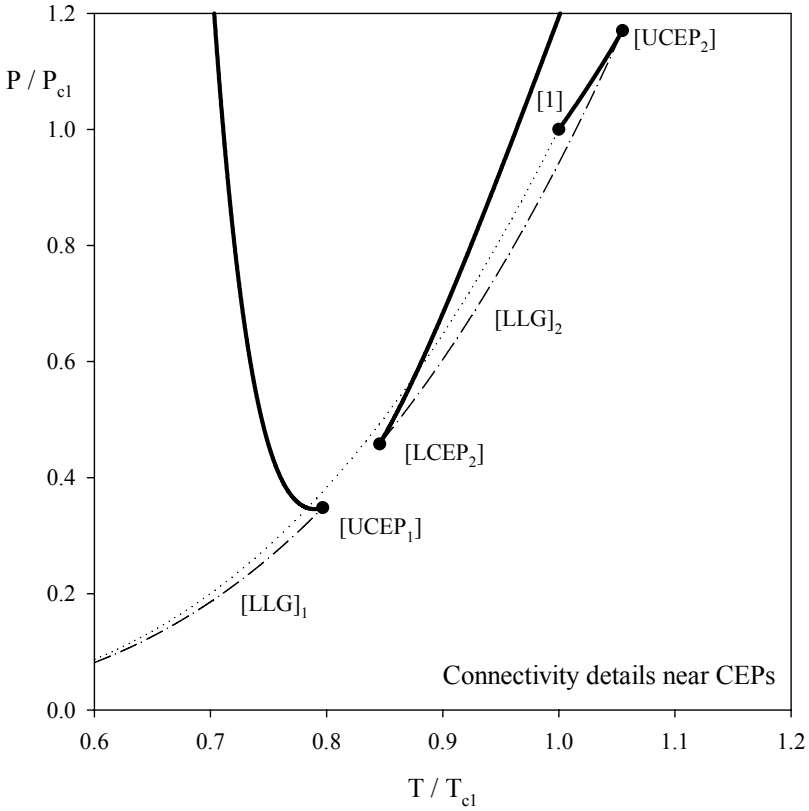

Fig. b

Figure 5

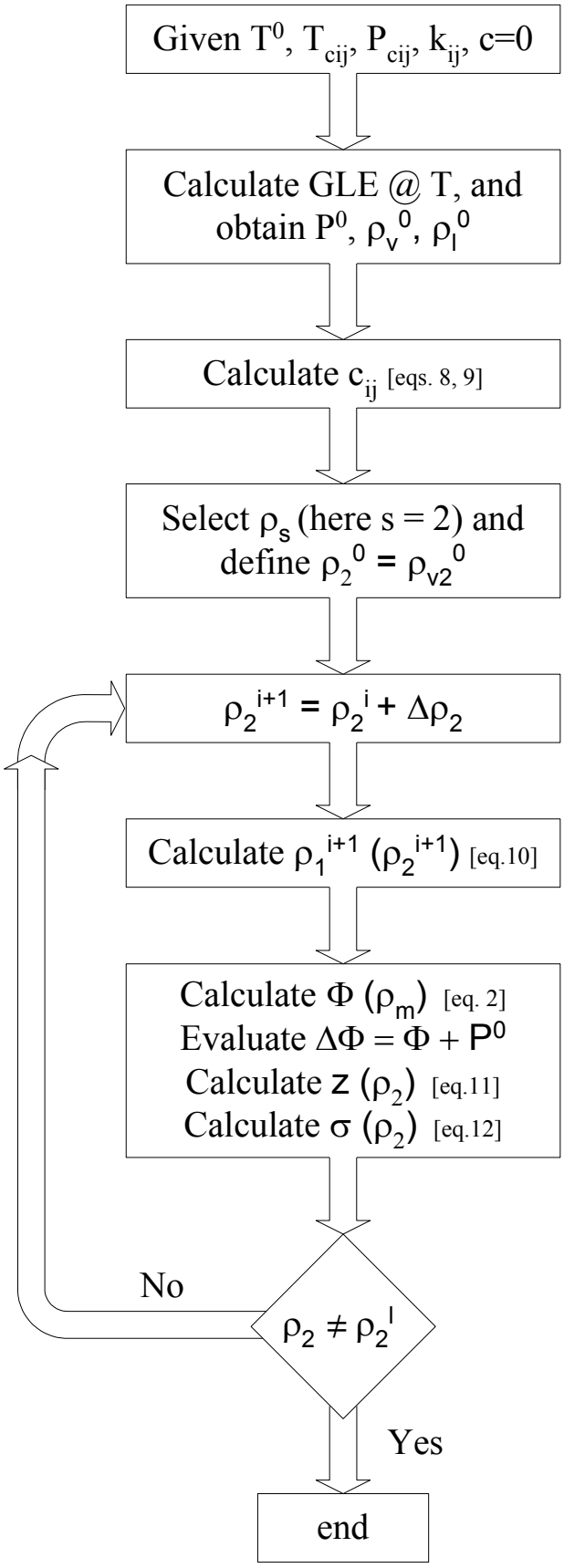
Given T^0, T_{cij}, P_{cij}, k_{ij}, c=0
Calculate GLE @ T, and obtain P^0, ρ_v^0, ρ_l^0
Calculate c_{ij} [eqs. 8, 9]
Select ρ_s (here s = 2) and define $\rho_2^0 = \rho_{v2}^0$
$\rho_2^{i+1} = \rho_2^i + \Delta\rho_2$
Calculate ρ_1^{i+1} (ρ_2^{i+1}) [eq.10]
Calculate Φ (ρ_m) [eq. 2]
Evaluate $\Delta\Phi = \Phi + P^0$
Calculate z (ρ_2) [eq.11]
Calculate σ (ρ_2) [eq.12]
No
$\rho_2 \neq \rho_2^l$
Yes
end

Figure 6

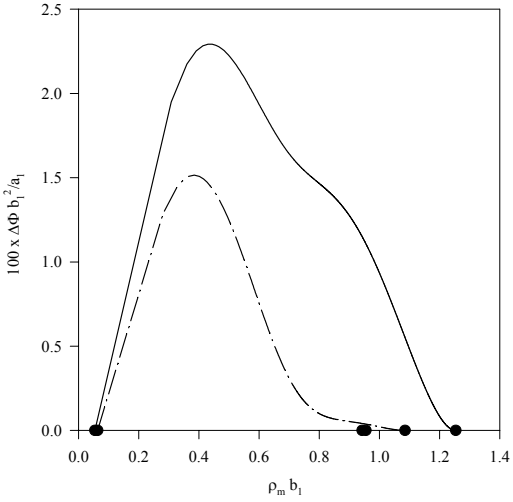

7.a $T / T_{c1} = 0.78$

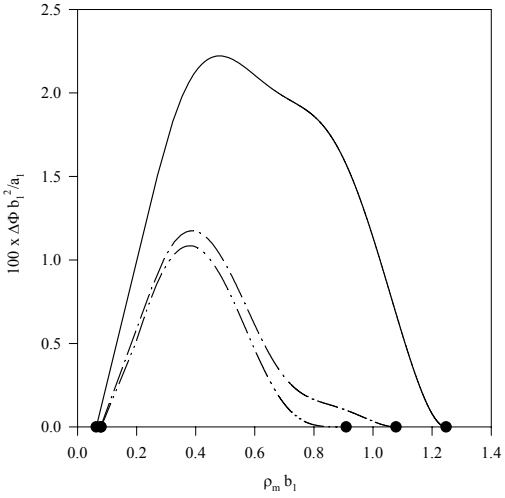

7.b $T / T_{c1} = 0.82$

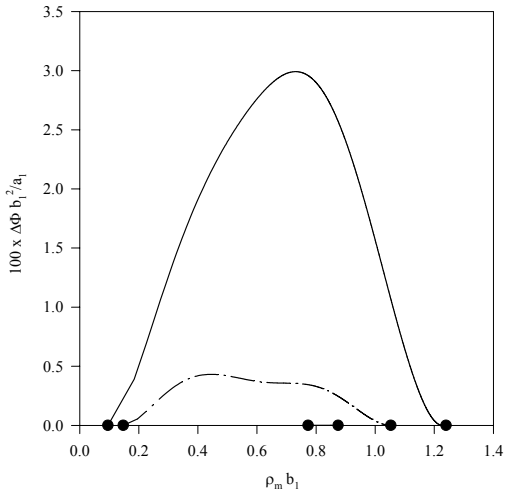

7.c $T / T_{c1} = 0.95$

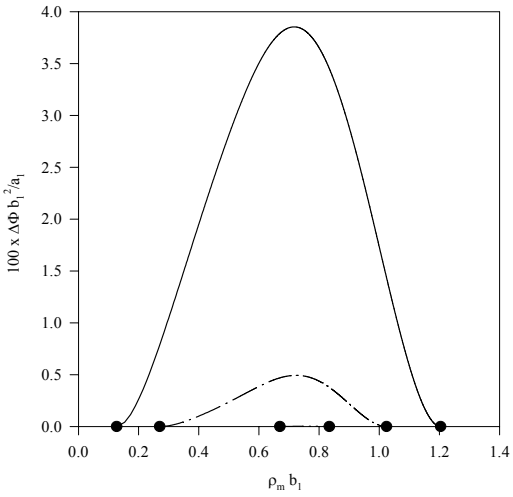

7.d $T / T_{c1} = 1.10$

Figure 7

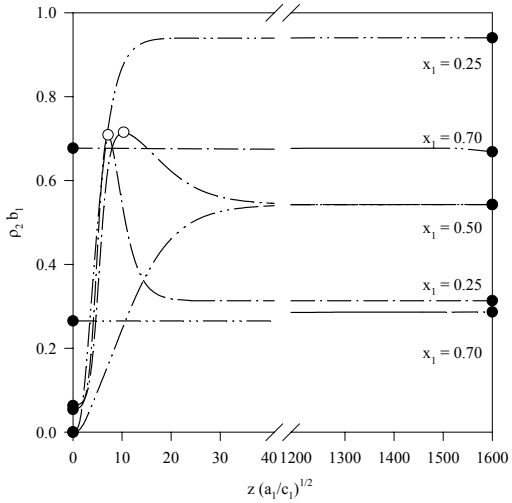

8.a $T / T_{c1} = 0.78$

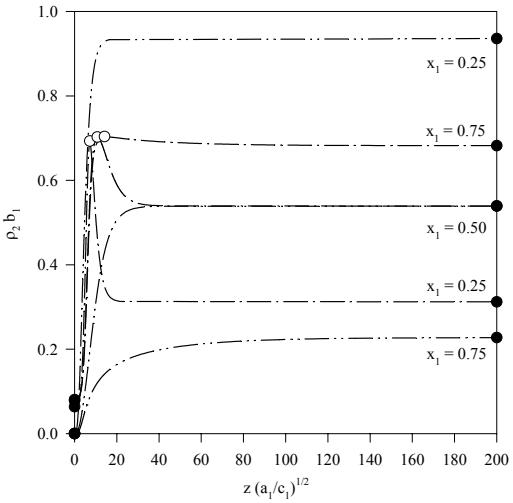

8.b $T / T_{c1} = 0.82$

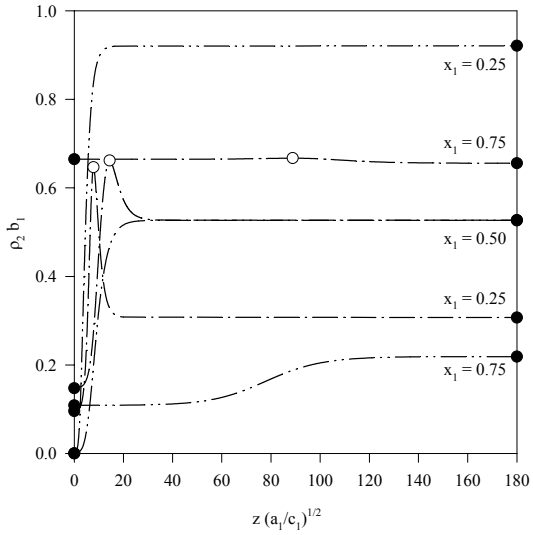

8.c $T / T_{c1} = 0.95$

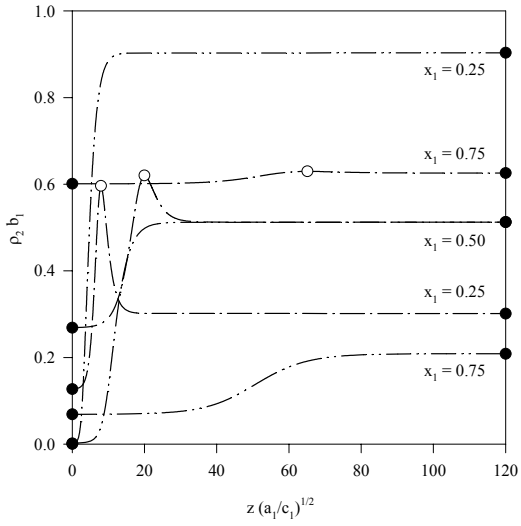

8.d $T / T_{c1} = 1.10$

Figure 8

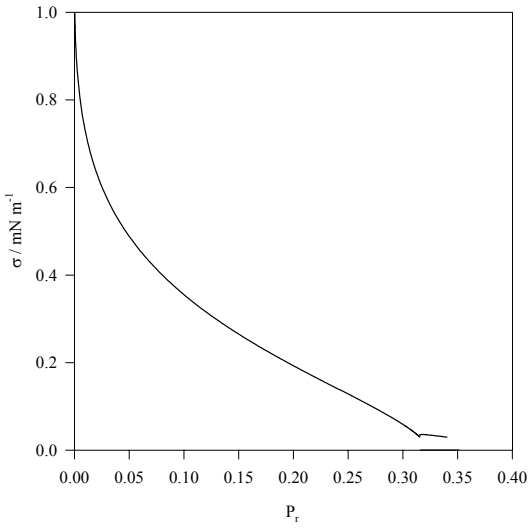

9.a $T / T_{c1} = 0.78$

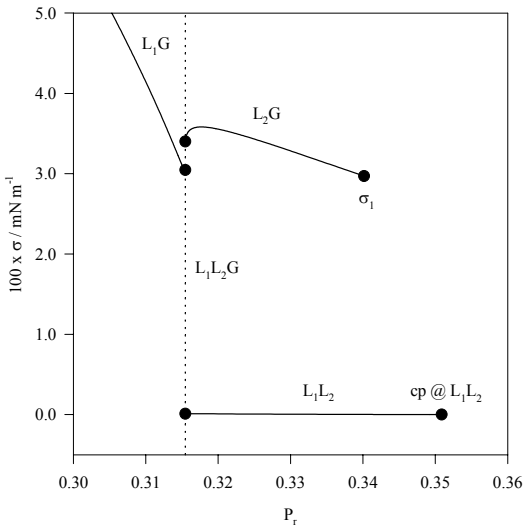

9.b $T / T_{c1} = 0.78$

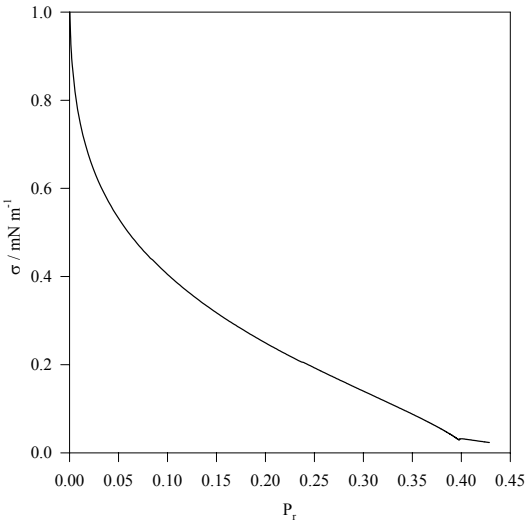

9.c $T / T_{c1} = 0.82$

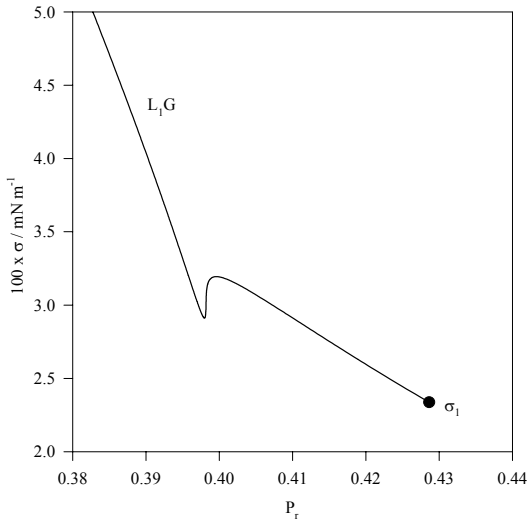

9.d $T / T_{c1} = 0.82$

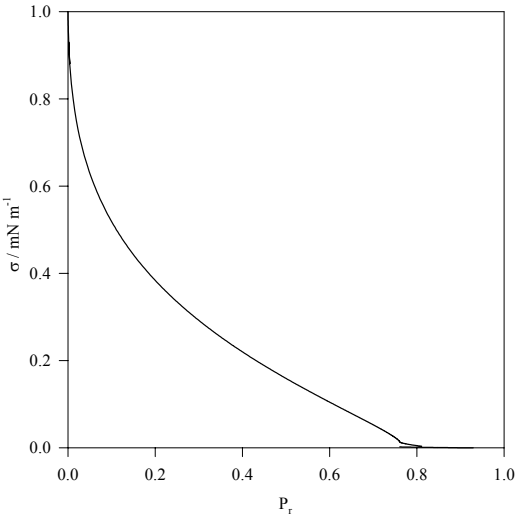

9.e $T / T_{c1} = 0.95$

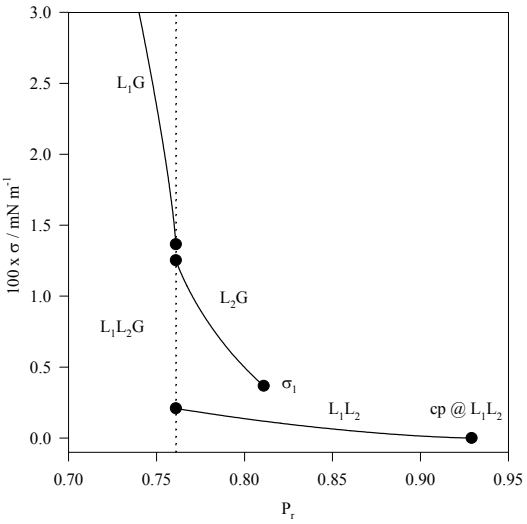

9.f $T / T_{c1} = 0.95$

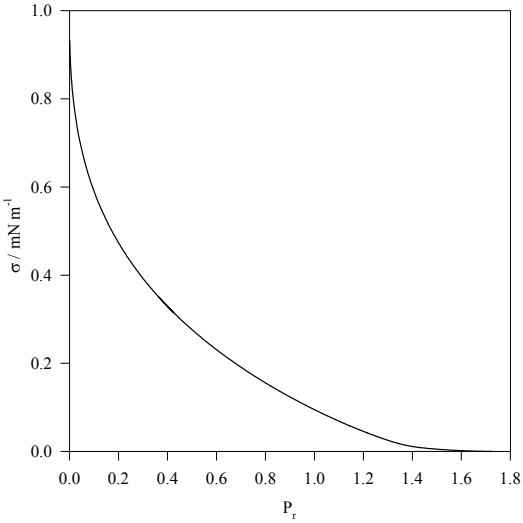

9.g $T / T_{c1} = 1.10$

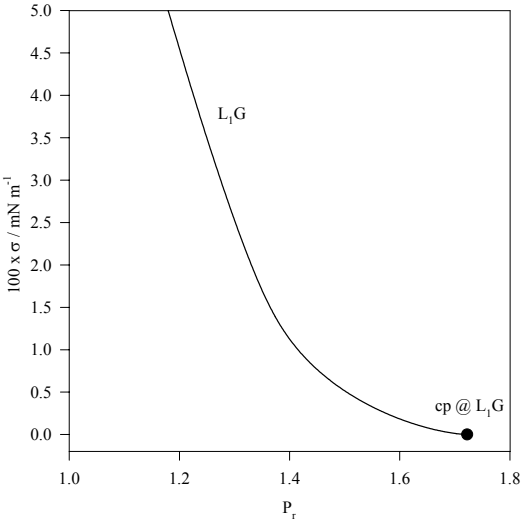

9.h $T / T_{c1} = 1.10$

Figure 9

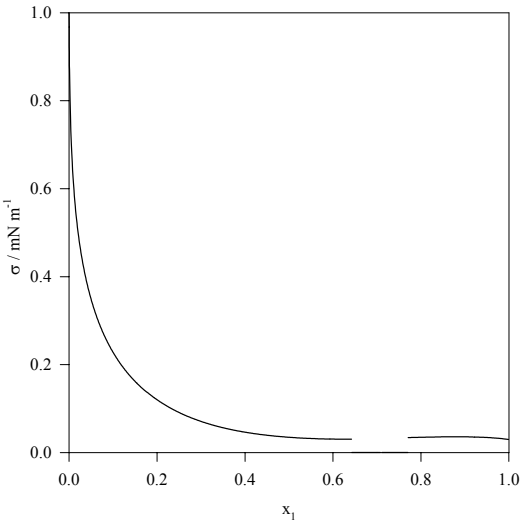

10. a $T / T_{c1} = 0.78$

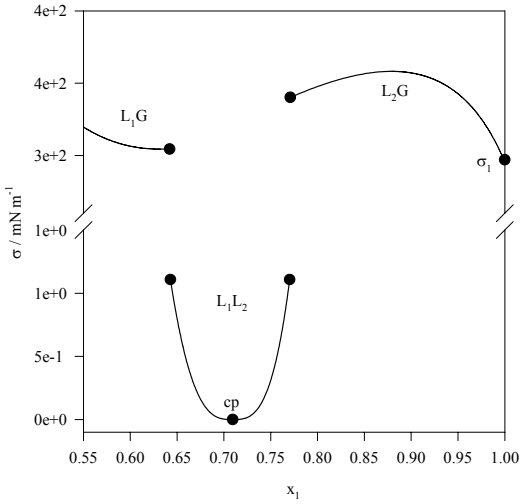

10.b $T / T_{c1} = 0.78$

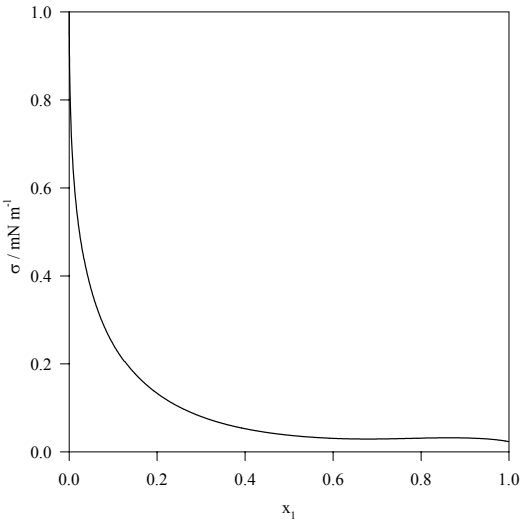

10.c $T / T_{c1} = 0.82$

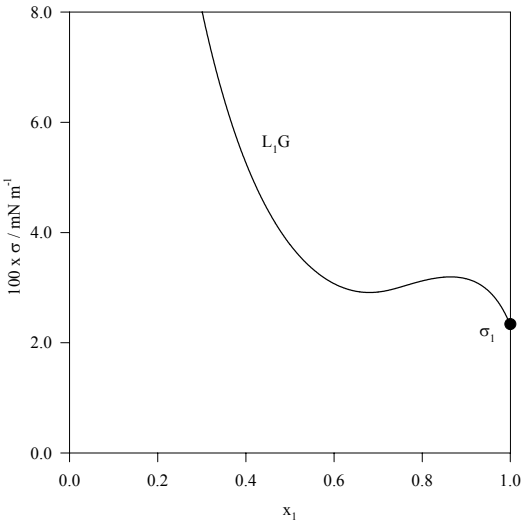

10.d $T / T_{c1} = 0.82$

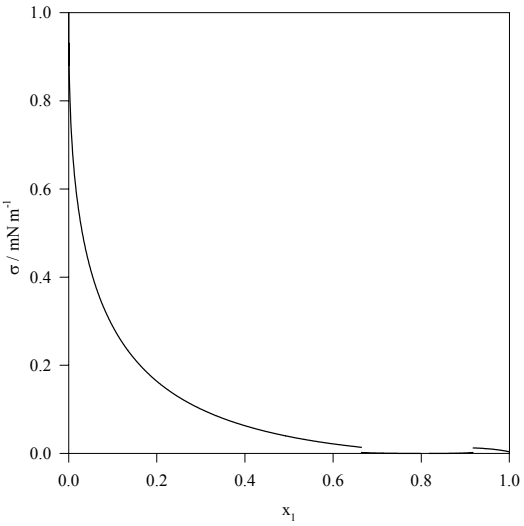

10.e T / T_{c1} = 0.95

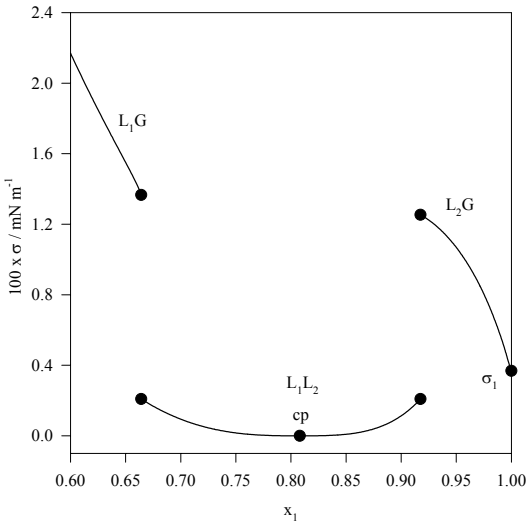

10.f T / T_{c1} = 0.95

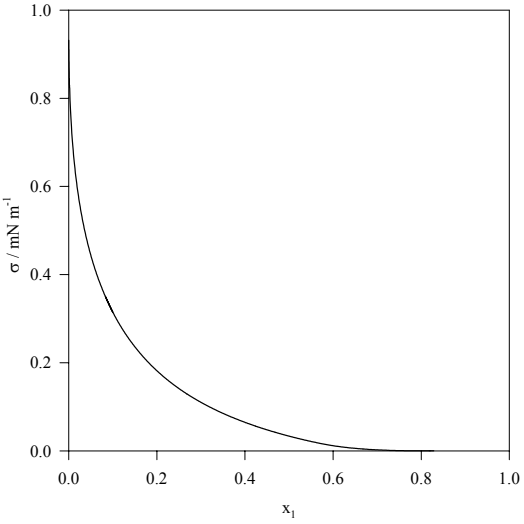

10.g T / T_{c1} = 1.10

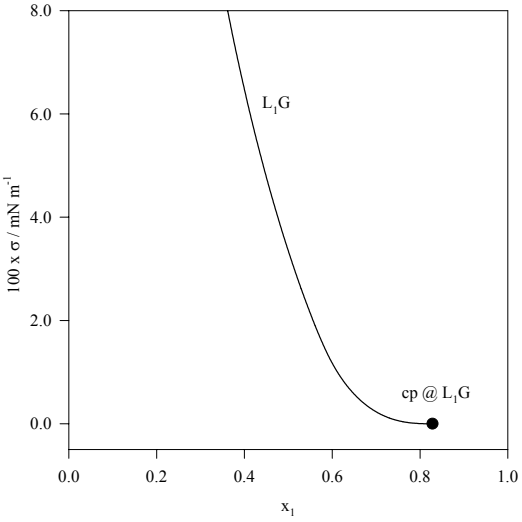

10.h T / T_{c1} = 1.10

Figure 10

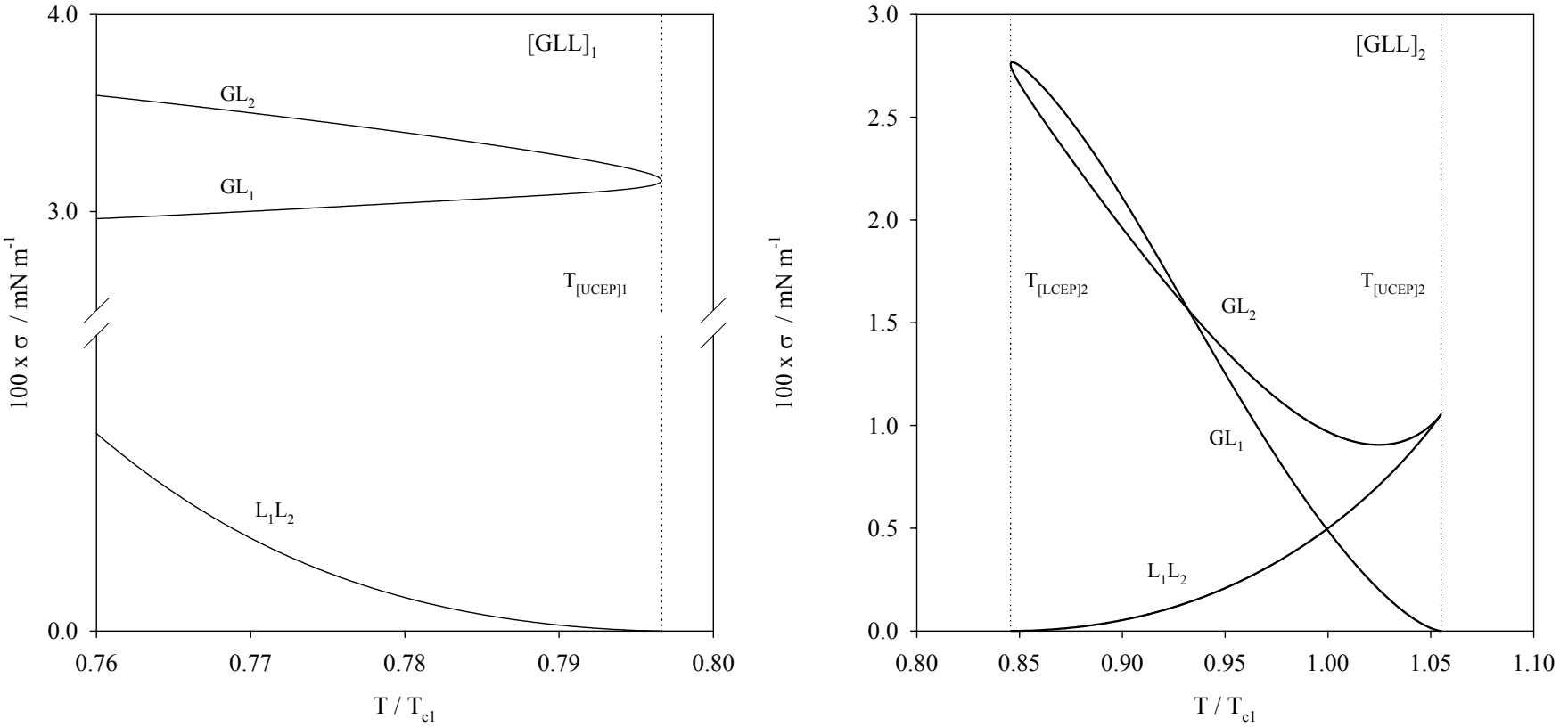
[GLL]1
GL2
GL1
T[UCEP]1
L1L2
100 x σ / mN m-1
T / Tc1
4.0
3.0
0.0
0.76
0.77
0.78
0.79
0.80
[GLL]2
T[LCEP]2
T[UCEP]2
GL2
GL1
L1L2
2.5
2.0
1.5
1.0
0.5
0.85
0.90
0.95
1.00
1.05
1.10

Figure 11